An optimized method for extracting slope length in RUSLE from raster digital elevation

Catena

Dong, Liang; Ge, Chenyu; Zhang, Hongming; Liu, Zihan; Yang, Qinke et al

https://doi.org/10.1016/j.catena.2021.105818

Catena 209 (2022) 105818

Contents lists available at ScienceDirect

Catena

journal homepage: www.elsevier.com/locate/catena

An optimized method for extracting slope length in RUSLE from raster digital elevation

Liang Dong [a], Chenyu Ge [a], Hongming Zhang [a,*], Zihan Liu [a], Qinke Yang [b], Bei Jin [c], Coen J. Ritsema [d], Violette Geissen [d]

[a] College of Information Engineering, Northwest A & F University, Shaanxi 712100, China
[b] Department of Urbanology and Resource Science, Northwest University, Shaanxi 710069, China
[c] College of Economics & Management, Northwest A & F University, Shaanxi 712100, China
[d] Soil Physics and Land Management Group, Wageningen University, Wageningen, the Netherlands

ARTICLE INFO

Keywords:
Soil erosion
RUSLE
Slope Length
GIS
Terrain analysis

ABSTRACT

The Universal Soil Loss Equation (USLE) and the Revised Universal Soil Loss Equation (RUSLE) have been widely used for predicting average soil loss. Slope length is an important topographical parameter of the L factor in USLE/RUSLE. Among the widely studied GIS procedures for extracting slope length, the distributed watershed erosion slope length (DWESL) based on the unit contributing area estimation method, which considers two-dimensional runoff process and cutoff factors, is a relatively complete model for calculating slope length. Slope length in the DWESL model is primarily calculated using conventional flow direction algorithms such as D8, Dinf, MS and MFD-md. However, DWESL outputs require further improvement due to the errors in the usual estimates of the uphill contributing area and the effective contour length of discrete elements. Combined with a theoretical differential equation of specific catchment area on hillsides, the calculation of the DWESL model was optimized without estimating the uphill contributing area or the effective contour length for each cell. The proposed integration method based on the topographical features slope line, contour curvature and cutoff factors (ITF method) was used to extract slope length from the raster digital elevation. Slope length extracted using the ITF method had the smallest error in verification of mathematical surfaces (average RRMSE = 0.0573), and its spatial distribution was more consistent with the structure of the terrain surface for all test data, relative to the conventional flow direction algorithms in the original DWESL model. The proposed ITF method could provide a reference for predicting soil erosion using the USLE/RUSLE model.

1. Introduction

The Universal Soil Loss Equation (USLE) (Wischmeier and Smith, 1978) and Revised Universal Soil Loss Equation (RUSLE) (Renard et al., 1991) have been widely used to predict annual average soil erosion due to their simplicity and robustness (Liu et al., 2002; Winchell et al., 2008; Panagos et al., 2015; Alexakis et al., 2019; Baghdad et al., 2020). The slope-length factor (L factor) in this model is the ratio between the loss of soil at any slope length and that loss from a 22.13 m length slope, considering the same soil type and slope gradient. Noted as,

$$L = \left(\frac{\lambda}{22.13}\right)^{m} \quad (1)$$

where m is a variable slope-length exponent and λ is slope length (m) defined as "the distance from the point of origin of overland flow to the point where either the slope gradient decreases enough that deposition begins, or the runoff water enters a well-defined channel that may be part of a drainage network or a constructed channel" (Wischmeier and Smith, 1978). The L factor has always been questioned because of the choice of slope length (Renard et al., 1991).

In the definition of slope length, λ can be calculated as the horizontal projection distance along the flow path (Mitasova et al., 1996) based on a digital elevation model (DEM). Hickey et al. (1994) developed a non-cumulative slope length method for pixel-by-pixel calculation using the principle of maximum slope, deterministic eight-neighbors(D8) algorithm (O'Callaghan and Mark, 1984). This method has been modified for identifying deposition by considering of the cutoff slope angle in the calculation of slope length (Hickey, 2000; Remortel et al., 2001). These

* Corresponding author.
E-mail addresses: lordong@nwafu.edu.cn (L. Dong), zhm@nwafu.edu.cn (H. Zhang).

https://doi.org/10.1016/j.catena.2021.105818
Received 4 May 2021; Received in revised form 31 August 2021; Accepted 18 October 2021
Available online 13 November 2021

early GIS procedures were implemented by Arc Macro Language programs, and a C++ executable with high execution efficiency was then developed (Remortel et al., 2004).

These flow-path-based cumulative length (FCL) methods mainly calculate each cell slope length (CSL) and accumulate them along a single flow path. FCL methods, however, do not account for the effect of flow convergence (Desmet and Govers, 1997; Winchell et al., 2008; Garcia Rodriguez and Gimenez Suarez, 2012). Moore et al. (1986) demonstrated that serious erosion and deposition are more likely to occur in areas of convergence and that the capacity of flow to transport sediment is lowest in divergent areas. Topographical divergence or convergence shows that the length of one-dimensional horizontal projection cannot transport sediment in overland flow well (Winchell et al., 2008; Fu et al., 2013; Zhang et al., 2017; Anjitha Krishna et al., 2019). The basic terms in USLE/RUSLE indicate that the L factor refers to the mean rate of erosion for an area with a length of λ (i.e. the length of the uphill horizontal projection) and a unit contour width in a field (Moore and Wilson, 1992; Desmet and Govers, 1997). Moore and Wilson (1992) therefore proposed replacing λ with specific catchment area (SCA), so the L factor could be calculated as,

$$L = \left(\frac{A_s}{22.13}\right)^m \tag{2}$$

where A_s (m^2/m) is the ratio of the uphill contributing area to the contour width.

Desmet and Govers (1996) then considered the sectional calculation of slope length (Foster and Wischmeier, 1974) and extended the approach using a GIS procedure in grid DEMs, in which the cell was the basic calculation unit for discrete regular DEM data (the unit contributing area-based (UCA) method). A_s for each grid is obtained by dividing the upstream accumulated area by the effective contour length of the cell (Costa-Cabral and Burges, 1994). The UCA method is thus further deduced to calculate the cumulative slope length for each cell (Zhang et al., 2013; Zhu et al., 2014; Yang, 2015). An integrated tool (LS-TOOL) was designed in a recent model to improve the UCA method and calculate the distributed watershed erosion slope length (DWESL) (Zhang et al., 2013; Zhang et al., 2017), in which the cutoff factors caused by deposition (i.e. slope cutoff) and well-defined channel networks (i.e. channel cutoff) are comprehensively considered based on the concept of Wischmeier and Smith (1978). Several studies (Zhang et al., 2013; Yang, 2015; Zhang et al., 2017; Brychta and Brychtová, 2020) then used flow-simulation algorithms to iteratively calculate the cumulative slope length of each cell due to the convenience of topology, such as the single-flow algorithm (SFA) D8 (O'Callaghan and Mark, 1984), the multiple-flow algorithm (MFA): Multiple-flow-direction based on slope (MS) (Quinn et al., 1991) and deterministic infinite-node (Dinf) (Tarboton, 1997).

The values of the slope length and the L factor based on the UCA method, however, are over- or underestimated in the verification of field tests (Desmet and Govers, 1996; Winchell et al., 2008; Zhang et al., 2013; Hrabalíková and Janeek, 2017; Zhang et al., 2017). In addition to the influencing factors such as DEM data accuracy (Yadav and Indu, 2016; Wang et al., 2016), resolution (Zhu et al., 2016; Wang et al., 2020) and the cutoff condition of the slope length (Zhang et al., 2013), in terms of the calculation model of the UCA method, the usual estimates of the uphill contributing area and the effective contour length of discrete elements are also considered to be the main causes of inaccuracies. UCA errors vary in all flow-simulation algorithms in theoretical verification (Zhou and Liu, 2002; Qin et al., 2007; Qin et al., 2013; Pilesjö and Hasan, 2014). Gallant and Hutchinson (2011, para.59) reported that assuming flow width (i.e. the length of effective contour) to be approximately equal to the cell size was problematic. A mathematical formula was derived for describing the nonlinear relationship between SCA and the contour curvature along the slope line (the differential equation for SCA) (Gallant and Hutchinson, 2011), which provides support for more accurate calculations but has not been widely used to extract slope length in grid DEMs.

The purpose of this study was to design an integrated method for more accurately extracting slope length. Combined with the differential equation for calculating SCA (Gallant and Hutchinson, 2011), we optimized the method for calculating slope length in the DWESL model proposed by Zhang et al. (2013). The new proposed integration method was based on topographical features (ITF method) using slope line, contour curvature and cutoff factors, avoiding the usual estimates of the uphill contributing area and effective contour length for each cell. We compared and analyzed the results extracted using the ITF method and the algorithms simulating conventional flow for mathematical surfaces and real terrain data, which could provide a reference for predicting average soil loss using the USLE/RUSLE model.

2. Methodology

2.1. Optimized theoretical DWESL model

The optimized theoretical DWESL model is based on the assumption that the terrain has continuous first and second derivatives, and the infiltration of overland water is not considered (Mitasova and Hofierka, 1993; Shary, 1995). The terrain can be expressed by Eq. 3 on plane $\mathbb{R}^2$, which has generality on the set of real numbers,

$$z = f(x, y) \tag{3}$$

where z is the continuous partial second derivative with no local minimum of depression. Let $z = c$, a constant that represents the elevation, hence $c = f(x, y)$ is the contour equation defined in the XOY plane. The slope line element is $dt(dX, dY)$ satisfying,

$$dt \times \nabla z = 0 \tag{4}$$

which is perpendicular to the contour. The X and Y components of the slope line element can be deduced as,

$$\frac{dY}{dX} = \frac{-1}{\frac{dy}{dx}} = \frac{-1}{-\left(\frac{f_x}{f_y}\right)} = \frac{f_y}{f_x} \tag{5}$$

The length of the slope line can be calculated using a linear integral equation along the element, so the formula for calculating the length of the slope line (l) from the start point (x_s, y_s) and terminal point (x_t, y_t) is,

$$l_{(x_t, y_t)} = \int_{x_t}^{x_s} \sqrt{1 + \left(\frac{f_y}{f_x}\right)^2} \cdot dx \tag{6}$$

The transport of overland material driven by gravity follows the descending direction of the gradient along stream tubes (Costa-Cabral and Burges, 1994). Slope lines provide a perfect match to the theoretical flow lines that nondispersive flows of water and sediments extend and represent the skeleton of the divergent flow pattern (Orlandini et al., 2014). A sketch map (Fig. 1) is used to illustrate the DWESL model. The start point of DWESL is usually the hilltop or a new start point after the cutoff position. The end point of DWESL is defined as the edge of the catchment or cutoff point, where the deposition caused by the saturated state of sediment transport caused by a change in slope is considered as the slope cutoff, which can be determined by calculating the rate of change in slope steepness along the extended direction of the slope line (Hickey, 2000; Remortel et al., 2001). The rate of change in gradient is a flexible parameter in different landforms, which will be determined in actual situations. The channel cutoff or other human interventions are priori information that requires an analysis of the real terrain.

As noted in Eq. 2, slope length is replaced by SCA, and A_s at a point is defined as,

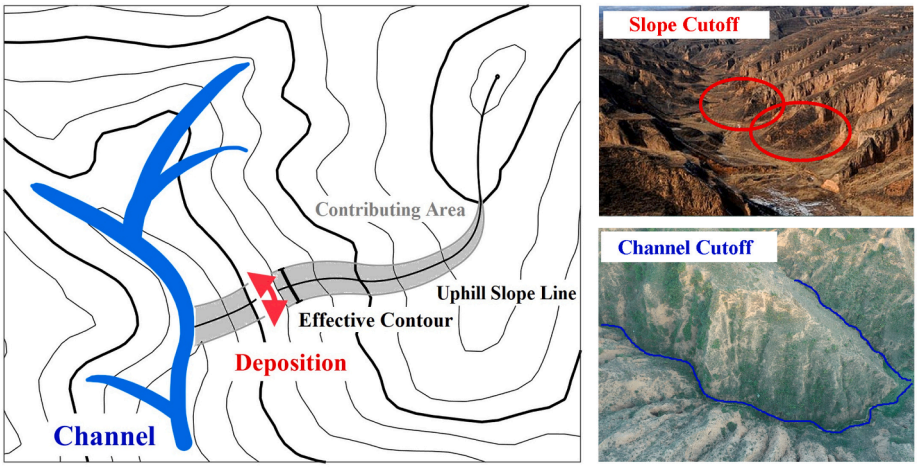

Fig. 1. Sketch map of the distributed watershed erosion slope length based on a specific catchment area and cutoff factors.

$$A_s = \lim_{w \to 0} \frac{A}{w} \tag{7}$$

where w is the width of the flow tube (i.e., the length of effective contour) and A is the uphill contributing area.

In the previous model (Zhang et al., 2013; Zhang et al., 2017), A_s of each cell in the grid DEM is used to calculate slope length based on the UCA method as,

$$A_{s_{i,j-out}} = \frac{A_{i,j-out}}{D_{i,j}} = \lambda_{i,j} \tag{8}$$

where $A_{i,j-out}$ (m^2) is the contributing area at the outlet of the grid cell with coordinates (i, j), $D_{i,j} = cellsize \cdot (|sin\theta_{i,j}| + |cos\theta_{i,j}|)$ is the effective contour length (m) of the corresponding coordinates and $\theta_{i,j}$ is the aspect direction for the grid cell with coordinates (i, j). Eq. (8) is further deduced because the contributing area of each cell can be represented as the sum of the contributing areas of the surrounding eight cells that flow into it. The slope length of each cell can then be obtained as,

$$\lambda_{i,j} = \sum_{x=0,y=0}^{x=i,y=j} \sum_{k=1}^{m} \lambda_{x,y} \tag{9}$$

where k is the direction code for the surrounding eight cells that could flow into the central grid, so $\lambda_{x,y}$ can be regarded as the CSL of each grid. The key of the previous model is therefore to use the flow-direction algorithm to calculate $\lambda_{x,y}$.

In the optimized theoretical DWESL model, according to Eq. 2, we combine the theoretical differential Eq. (10) of SCA to calculate the slope length, which is described as the rate of change of A_s to l (Gallant and Hutchinson, 2011, para.28),

$$\frac{\partial A_s}{\partial l} = 1 - A_S \cdot k_c \tag{10}$$

where k_c is curvature of contours. We can obtain A_s for any point along the uphill slope line for calculating DWESL using Eq. 6 and Eq. 10 as long as the location of the cutoff point has been determined.

2.2. Calculation of DWESL in grid DEMs

2.2.1. Calculation processes

The solution and method of numerical approximation of the parameters in the model based on the theoretical DWESL model are described in detail in the next sections. The complete procedure for calculating DWESL mainly consists of the following steps (Fig. 2).

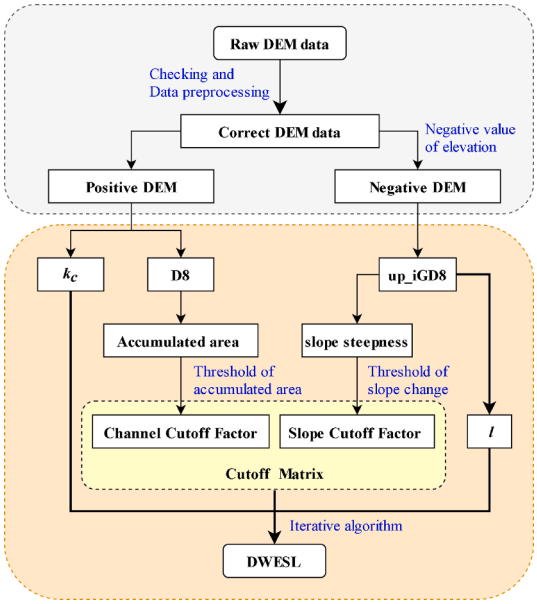

Fig. 2. Flowchart of the procedure for calculating DWESL.

Step 1: Data preparation. Spurious sinks generated due to the process of interpolation, generalization, and so forth during the production of the DEM blocks (Yan et al., 2018). We firstly should check the raw data and fill all spurious sinks with a routine iterative method (Remortel et al., 2004), including interior nodata cells and isolated local depressions (pixel-sized) (Zhang et al., 2017). The corrected DEM was obtained after above data preprocessing. Then, the corrected DEM (positive DEM) is flipped to get negative DEM by taking a negative value of elevation, which will provide data support for subsequent calculations.

Step 2: Calculate D8 and k_c (Section 2.2.4) with positive DEM, and calculate up_iGD8 (Section 2.2.2) and slope steepness with negative DEM.

Step 3: Calculate l (Section 2.2.2) and the slope cutoff factor (Section 2.2.3) using up_iGD8.

Step 4: Use D8 to calculate the accumulated area to determine the channel cutoff factor (Section 2.2.3).

Step 5: Use up_iGD8, l, k_c and the cutoff matrix (including slope cutoff factor and channel cutoff factor) to calculate DWESL (Section 2.2.4).

2.2.2. Calculation of the length of the uphill slope line

The length of the uphill slope line (l) in Eq. 6 and Eq. 10 is the distance from the point of interest to the top of the hill perpendicular to the contour. The numerical integration requires very complex and meticulous calculations when interpolating a DEM to place the slope line as close to the center of the grid as possible (Gallant and Hutchinson, 2011, para.50). Qin et al. (2017) thus designed parallel calculation methods to improve efficiency. For more convenient application, a suitable SFA based on grid DEMs is adopted in the ITF method.

The classical D8 algorithm is a greedy strategy for determining the direction with the largest local difference in elevation at each step, which will lead to more deviations compared to the exact slope line. D8 with least transversal deviation algorithm (D8-LTD) was firstly proposed to correct the deviation between D8 and the exact slope line (Orlandini et al., 2003; Orlandini et al., 2014), the path with the minimum error between the exact slope line can be obtained by adjusting the deviation parameters of each single path. But the parameters of correction for this method cannot dynamically adapt to the global calculation, thus the improved global D8 algorithm (iGD8) (Shin and Paik, 2017) was proposed. iGD8 did not need to individually adapt to every slope line of the surface, and obtained almost the same result as D8-LTD using global optimal solution, which is simple and good performance. Recently an improved flow aggregation D8 based algorithm (iFAD8) (Wu et al., 2020) used more upstream information and set dynamic damping factors for determining the downstream direction of each cell. iFAD8 optimized the shortcomings of other SFAs in theory but more complex calculations made the application more difficult. In terms of the performance and operability of these algorithms, iGD8 is a relatively good choice for this work. The SFAs require each cell to extend in a unique downstream direction, which causes some cells on the convex hillside to lose their upstream source and affects the calculation of cumulative length (illustrated in Fig. 3a). In contrast, SFAs can effectively converge and extend to the lowest local point on a concave hillside. Although we can reverse the calculation to get the backtracking runoff trajectory by modifying the algorithm, the more convenient way for calculating uphill l using SFAs is thus to flip the terrain by taking a negative value of elevation to obtain negative DEM data, which ensures that each point of interest has a continuous path to the real hilltop or local maximum (illustrated in Fig. 3b).

We chose to use iGD8 (available from website of Shin and Paik (2017), http://river.korea.ac.kr) for determining the uphill direction of each cell based on negative DEM data (named up_iGD8) and then calculated the summation length along the path of up_iGD8. SFAs with deviation correction, however, repeatedly deform the slope line, and the summation of the distance of each segment (1 or $\sqrt{2}$·*cellsize*) between adjacent cells causes a large error. Paz et al. (2008) thus multiplied each line segment by 0.962 based on statistical results to reduce the error of cumulative length. We proposed a strategy to correct the calculation of cumulative length by merging local segments. The correction is illustrated in Fig. 3c. A local path consisting of every three segments was replaced with the Euclidean distance, and the other segments were accumulated normally. This strategy can help reduce the excess length of up_iGD8 in zigzag paths and ensure that pure straight paths are not influenced.

2.2.3. Determination of the cutoff factors

The description of the cutoff factors in the definition of slope length referred to the possible hindrance of sediment transport, including deposition (Slope cutoff) and partition (channel cutoff or other human interventions). According to the DWESL model, the slope length was stopped and re-accumulated at these possible cutoff positions, in which slope cutoff and channel cutoff were mainly considered in practical calculations.

Slope cutoff factor: Different landforms have different soil types, so the threshold of slope cutoff may differ during sediment transport. The Chinese Soil Loss Equation (Liu et al., 2002) generally recommends that the threshold of change in gradient be 70% when the slope is $<2.86°$ and

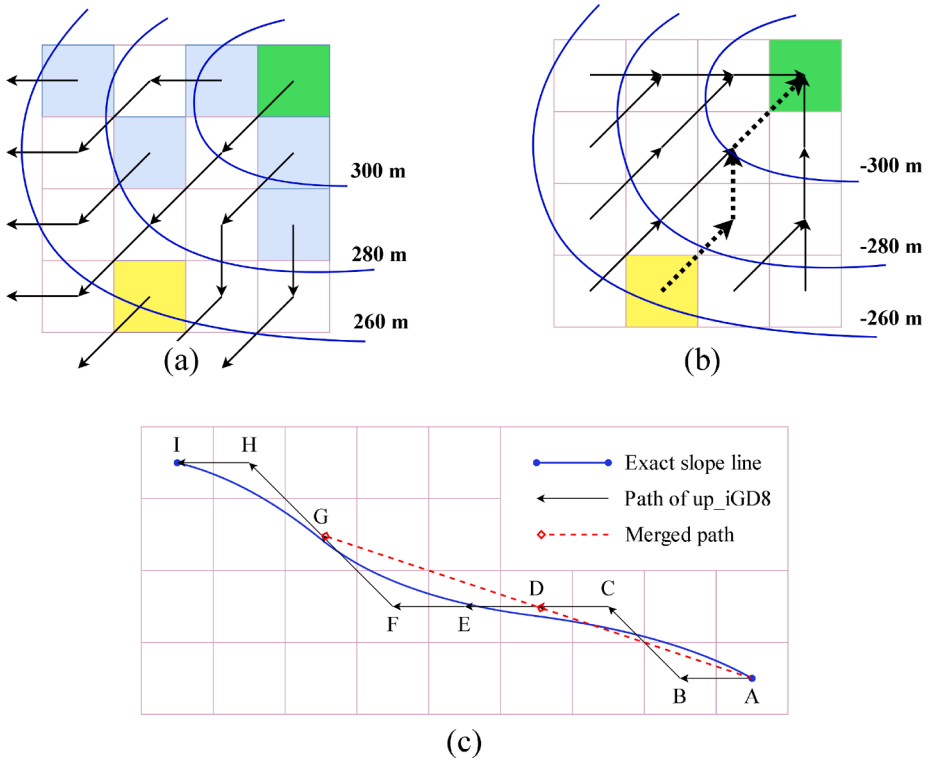

Fig. 3. (a) The cells lost their upstream source on the convex slope using SFA, so their uphill slope lines are incomplete. (b) Calculate the uphill slope line using negative DEM and SFA, thus each cell has a complete uphill slope line. (c) Schematic for calculating the length of the uphill slope line. Local segments (AB, BC and CD) are merged into AD, segments DE, EF and FG are merged into DG and the cumulative length is calculated as $(\sqrt{10} + \sqrt{10} + \sqrt{2} + 1)$·*cellsize*.

50% when the slope is ⩾2.86°.

The position of the slope cutoff can be determined by calculating the rate of change in slope steepness along the direction of extension of the slope line. The uphill direction of each cell is obtained using up_iGD8 in Section 2.2.2, and the slope angle can also be calculated. To obtain the downhill slope cutoff position of each cell, we calculated the change in gradient of the eight neighboring cells that could point to the center. If the change in gradient from a neighboring cell to the central cell is larger than the corresponding threshold, the location of the neighboring cell is recorded and stored in the cutoff matrix.

Channel cutoff factor: Due to factors such as the magnitude and intensity of rainfall, the areas affected by net soil erosion and effective sediment transport are different in the catchment (López-Vicente et al., 2020). Overland flow and sediment from hillslopes may extend downstream along the gullies, ephemeral streams within the basin, which have not yet formed a well-defined channel. When enough runoff was gathered into a well-defined channel, sediment was also transported into the channel network and then gradually transported out or still stranded in the catchment. According to the definition of slope length, the accumulation of slope length in the above process should be stopped at the well-defined channel, otherwise the huge cumulative value will lose its quantitative significance (Renard et al., 1991).

Hence, the key is to determine the channel network. One of the conventional channel network extraction methods is to calculate the catchment area, which is the most direct and robust method. When the catchment area in the basin reaches the user-defined threshold, the cells in the channel network are considered to be the position of the channel cutoff. The accumulated area is calculated using a simple algorithm simulating flow (D8), and the iterative process uses the LS-TOOL method (forward-and-reverse traversal).

A reasonable channel cutoff threshold greatly influences the extracted slope length. The smaller the threshold is, the denser the extracted channel network is, and the cutoff position will expand to more streams, gullies and even convergent hillslopes. For the DEM data obtained at a certain time, the primary task is to extract the possible channels from morphology. Based on previous studies (Zhang et al., 2017), we combined the DEM with a Google image to mark the channel heads to further determine the threshold of accumulated area. When the accumulation of the cell is larger than the threshold, its position is recorded in the cutoff matrix.

2.2.4. Iterative algorithm of DWESL

The implicit requirement of the general solution to the differential Eq. (10) in the calculation is more stringent, so the general solution is no longer applicable when k_c along the slope line changes sign (Gallant and Hutchinson, 2011, para.38). In order to apply Eq. 10 to calculate DWESL for each point of interest, each cell is numerically integrated along the segment of the slope line, starting from 0 at the hilltop for piecewise calculation along the aspect of the cell. In this case, the approximate solution of Eq. 10 is used (Gallant and Hutchinson, 2011, para.40),

$$A_s(l) = \frac{1}{k_c} - \left(\frac{1}{k_c} - A_{s0}\right) e^{-k_c \cdot l} \tag{11}$$

The following principles (Gallant and Hutchinson, 2011, para.47,48) should be noted when using Eq. 11: Firstly, if $|k_c| < 10^{-4}$, the cell is on an almost plate-liked hillside, and Eq. 11 is calculated as,

$$A_s(l) = A_{s0} + l \tag{12}$$

Secondly, if $k_c > 20$, Eq. (13) is used to prevent the loss of accuracy caused by subtraction in Eq. 11,

$$A_s(l) = \frac{1}{k_c} \tag{13}$$

where A_{s0} is SCA at the top of the slope line segment, l is the length of the part of the slope-line segment under the direction of up_iGD8, and k_c of each cell is calculated using a differential formula. The second derivative of the central grid is calculated in 5 × 5 DEM windows (Fig. 4), and k_c is calculated as,

$$\begin{cases} k_c = \dfrac{-q^2 r + 2pqs - p^2 t}{\left(p^2 + q^2\right)^{3/2}} \\ p = \dfrac{\partial z}{\partial x} = \dfrac{z_3 + z_6 + z_9 - z_1 - z_4 - z_7}{6d} \\ q = \dfrac{\partial z}{\partial y} = \dfrac{z_1 + z_2 + z_3 - z_7 - z_8 - z_9}{6d} \\ r = \dfrac{\partial_z^2}{\partial x^2} = \dfrac{z_{x3} + z_{x6} + z_{x9} - z_{x1} - z_{x4} - z_{x7}}{6d} \\ s = \dfrac{\partial_z^2}{\partial x \partial y} = \dfrac{z_{x1} + z_{x2} + z_{x3} - z_{x7} - z_{x8} - z_{x9}}{6d} \\ t = \dfrac{\partial_z^2}{\partial y^2} = \dfrac{z_{y1} + z_{y2} + z_{y3} - z_{y7} - z_{y8} - z_{y9}}{6d} \end{cases} \tag{14}$$

When up_iGD8 of each cell is calculated in Section 2.2.2, the positions of the hilltop will be determined (i.e. the cell that cannot point to the neighbors). Eqs. (11)–(13) are used for iterative calculation to update $A_s$at the end of the slope line segment, a hierarchical traversal is carried out from each hilltop in turn and the cutoff point is then determined to calculate the DWESL of each cell. The specific implementation is:

1. set up an auxiliary queue starting from the hilltop,
2. search for eight neighbors that can point to the current cell, queue them and use Eqs. (11)–(13) to calculate the SCA of the cell,
3. determine whether the neighbors in step 2 are downstream of the cutoff point and stop accumulating,
4. follow steps 2 and 3 to search for the eight neighbors, then delete the current cell from the queue and update the first element of the queue,
5. perform steps 2–4 in turn until all connectable grids starting from the hilltop are processed, and
6. change the next hilltop as the first element of the queue and continue to calculate other cells following steps 2–5.

We implemented the algorithm in an object-oriented method (Algorithm 1). Each cell is assigned two attributes, A_s of the current cell and the cutoff information (*CUT*) from upstream. A value of *CUT* equal to zero indicates no cutoff, and a value of $CUT > 0$ indicates that the cutoff is in the upstream position, then stop accumulating. *CUT* is transferred downstream in an iterative process.

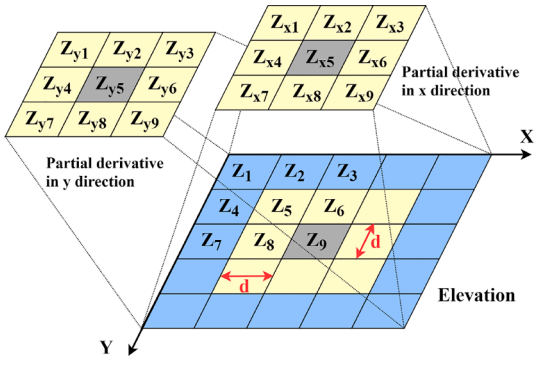

Fig. 4. Corresponding calculation unit in Eq. 14, where d is cell size.

Algorithm 1. Iterative calculation of DWESL

Input: *up_iGD8, l, k_c, Cutoff Matrix.*
01: Initialization: *AllCells.CUT* = 0, *AllCells.DWESL* = 0.
02: **for** $i \leftarrow 1$ **to** *DEM.row*
03: **for** $j \leftarrow 1$ **to** *DEM.column*
04: **if** *Cell (i. j)* point to Null **then**
05: Queue.push (*Cell (i, j)*)
06: **while** Queue is not empty **do**
07: **for** $k \leftarrow 1$ **to** 8 **do**
08: **if** *Next_Cell* point to *Current_Cell* **then**
09: Queue.push (*Next_Cell*)
10: calculate *Next_Cell.*A_s using Eqs. (11) to (13)
11: **if** *Current_Cell* is in *Cutoff Matrix* **then**
12: *Current_Cell.CUT* ← *Current_Cell.*A_s
13: **end if**
14: *Next_Cell.DWESL* ← *Next_Cell.*A_s - *Current_Cell.CUT*
15: *Next_Cell.CUT* ← *Current_Cell.CUT*
16: **end if**
17: **end for**
18: Queue.pop (*Current_Cell*)
19: **end while**
20: **end if**
21: **end for**
22: **end for**
Output: *AllCells.DWESL*

3. Experiment

3.1. Experimental data

3.1.1. Synthetic surfaces

We simulated the terrain using 10 mathematical surfaces. The original formulas of the synthetic surfaces are provided in Table 1. The theoretical DWESL of nine simple and regular artificial surfaces can be obtained. These surfaces included three types adapted from Wu et al. (2020), plate, divergent and convergent, each of which have three variants, planar, concave and convex (Fig. 5a-i). The last Himmelblau-Orlandini surface (Orlandini et al., 2014) could simulate the relatively complex surface, with four local hilltops, three saddles and a flow convergence area. The whole was a small catchment basin, which was used to compare the DWESL extracted from the compound hillslopes (Fig. 5j).

3.1.2. Real terrain data

Real terrain data were obtained from the XianNanGou catchment in the northwestern part of the Loess Plateau of China. The geographical location of the experimental sample area and the 3D surface were shown in Fig. 6, which was a hydrologically corrected DEM data set at a resolution of 5 m without depressions or flats (Yang et al., 2007).

3.2. Selection of algorithms for comparison

We compared the ITF method with four typical algorithms simulating flow to extract DWESL, including the deterministic eight-neighbors algorithm (D8) (O'Callaghan and Mark, 1984), the deterministic infinite-node algorithm (Dinf) (Tarboton, 1997), the multiple-flow-direction slope-based algorithm (MS) (Quinn et al., 1991) and the multiple-flow-direction based on the maximum downslope gradient algorithm (MFD-md) (Qin et al., 2007). CSL and the iterative calculation of these flow-direction algorithms were implemented using LS-TOOL (Zhang et al., 2013; Zhang et al., 2017) and its methods, equations Eq. 7 and Eq. 8.

3.3. Reference Values and Assessment

The thresholds of cutoff factors in mathematical surfaces have no realistic references, so we did not consider cutoff factors in extracting DWESL from the synthetic surfaces, and the main purpose was to compare and analyze the differences between the ITF method and the flow simulation algorithms in the spatial patterns and statistical results.

Without considering cutoff factors, the theoretical value of DWESL can be derived from Eq. 10 for the simple surfaces of plates, divergent cones and convergent inward cones,

$$\begin{cases} A_s(l) = A_{s0} + l, k_c(l) = 0; \\ A_s(l) = \dfrac{l}{2}, k_c(l) = \dfrac{1}{l}; \\ A_s(l) = \dfrac{l(2R-l)}{2(R-l)}, k_c(l) = \dfrac{1}{l-R}. \end{cases} \tag{15}$$

where R is the radius of the cone, which is excluded from consideration when $l = R$. Eq. (6), (15)the formulas of nine simple surfaces indicated that the theoretical values of the same type in planar, concave and convex are equal, because $l$does not change in the three styles of same type. In the above surfaces, the relative root mean square error (RRMSE) (Wechsler and Kroll, 2006) was used to evaluate the error between the results of these extraction methods and the theoretical values. RRMSE is calculated as,

$$RRMSE = \sqrt{\frac{1}{n}\sum_{i=1}^{n}\left(\frac{c_i - T_i}{T_i}\right)^2} \tag{16}$$

where c_i is the calculated result of each cell, and T_i is the theoretical value at the corresponding position.

Without an analytical solution of DWESL for all cells on Himmelblau-Orlandini surface, we selected sample points along the slope line on the hillside to evaluate the DWESL error. The reference values on Himmelblau-Orlandini surface were calculated strictly according to Eq.

Table 1
Parameters of the synthetic surfaces.

Synthetic surfaces		Original formula	Limits
Plate	Planar	$z_1 = 0.1x + 0.2y$	$x \in [0, 50]$ $y \in [0, 25]$ $z_i \in \begin{cases} [0,10], i = 1,2,3 \\ [0,25], i = 4,5,7,8 \\ [0,15], i = 6,9 \end{cases}$
	Concave	$z_2 = 0.1z_1^2$	
	Convex	$z_3 = \sqrt{10z_1}$	
Divergent	Planar	$z_4 = 25 - \sqrt{(x-25)^2 + (y-25)^2}$	
	Concave	$z_5 = \dfrac{25z_4}{100 - 3z_4}$	
	Convex	$z_6 = 65 - \sqrt{2500 + 1875(1 - \frac{z_4}{25})^2}$	
Convergent	Planar	$z_7 = 25 - z_4$	
	Concave	$z_8 = 25 - z_5$	
	Convex	$z_9 = 15 - z_6$	
Himmelblau-Orlandini		$z_{10} = 45 - 0.075[\{(\frac{x-25}{5})^2 + (\frac{y-25}{5}) - 4\}^2 + \{(\frac{y-25}{5})^2 + (\frac{x-25}{5}) - 7\}^2]$	$x \in [0, 50]$ $y \in [0, 50]$ $z_{10} \in [-10, 45]$

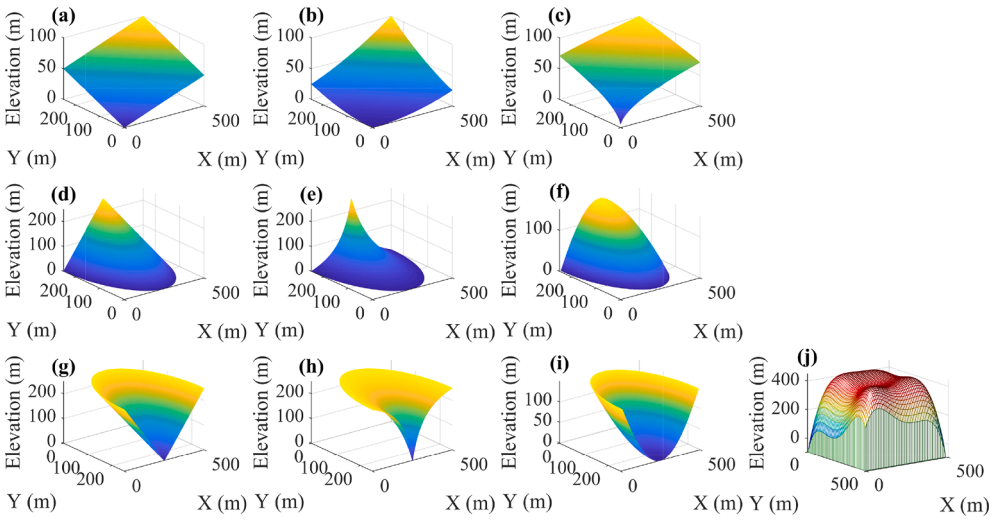

Fig. 5. 3D views of the synthetic surfaces. (a) Planar plate, (b) concave plate, (c) convex plate, (d) planar cone, (e) concave cone, (f) convex cone, (g) planar inward cone, (h) concave inward cone and (i) convex inward cone. (j) Himmelblau-Orlandini surface with four local hilltops, three saddle points and a flow-convergence area. (Note: the above continuous surfaces were discretized into raster data at an interval of 0.1 and then enlarged tenfold as a whole. The resolution of the synthetic surfaces was thus 1 m.).

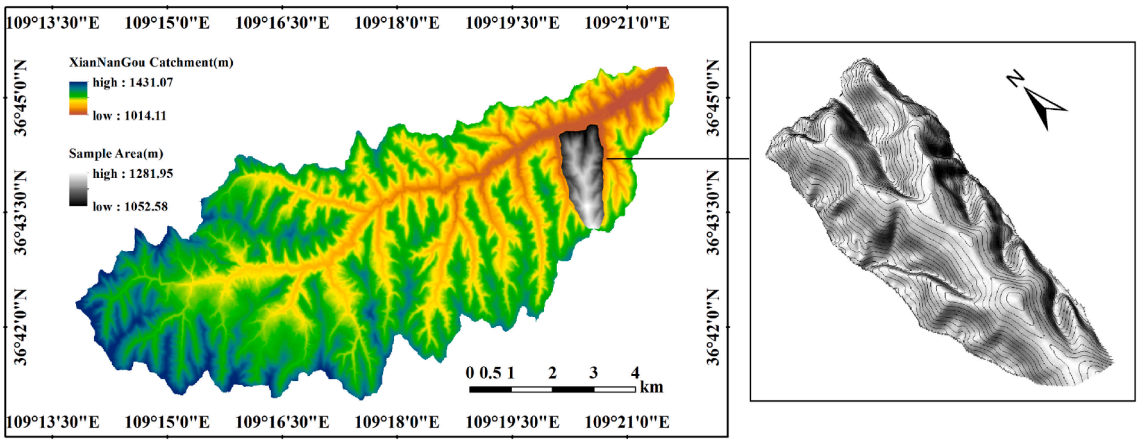

Fig. 6. Geographical location and 3D surface of the area from which the real terrain data were obtained.

(6) and (14) in the theoretical model. Runge–Kutta formula was used to calculated linear integral, which has been integrated into MATLAB's ode23tb solver (Orlandini et al., 2014).

Evaluating the performance of the algorithms using field observations for the actual terrain data is difficult (Bircher et al., 2019). In previous studies, the researchers manually measured the linear length along the vertical contours on the map to obtain the reference values of flow-path-based slope length (Zhu et al., 2016), another assessment based on statistical test was to look up values for LS factor from slope and horizontal slope length based on low ratio of rill to interrill erosion (Yang, 2015). These manual methods were not objective enough, and the reference values obtained were uncertain (Desmet and Govers, 1996). Especially for pixel level recognition, field test could only be carried out on a limited gentle slope, not anywhere in the catchment (Hrabalíková and Janeek, 2017). Most observations are based on visual or qualitative assessments (Garcia Rodriguez and Gimenez Suarez, 2012; Fu et al., 2013). In this work the above methods were no longer applicable because of the difference in the theoretical model of slope length. Hence, we mainly verified the rationality and precision of the proposed method on the mathematical surfaces, then tested the method in the actual terrain to analyze the spatial pattern and data distribution of the results.

4. Results and Discussion

4.1. Results of DWESL on synthetic surfaces

4.1.1. Theoretical and extracted slope lengths on nine simple surfaces

The spatial patterns of DWESL extracted from the planar, concave and convex styles of same type were very similar, so we chose all planar styles for illustration (Fig. 7).

The direction of D8 is limited to multiples of 45°, and the greedy-selection strategy of local maximum downslope is not well adapted to be perpendicular to the contours. The spatial pattern of D8 was obviously offset from the theoretical results. The local drainage direction of Dinf can effectively determine the weights assigned to the two neighborhood cells, and the spatial distribution approximates the theoretical results by cross-compensating the two directions. The spatial distribution of MS with complete divergence simulation ability changes gradually, but the cross-compensation in multiple directions renders the cumulative slope length obviously larger than the theoretical value. MFD-md with adaptive variation of flow distribution weight can simulate the effects of SFD and MFD. In the extraction results of the plate surface, the trend in direction of MFD-md is between that of D8 and MS, and its cumulative result is smaller than that of MS. The ITF method is based on up_iGD8 for determining the trend perpendicular to the contours. When $k_c = 0$, the theoretical derivation of DWESL ensures the validity of the results, and the spatial distribution is highly similar to the theoretical value on the plate surface (Fig. 7).

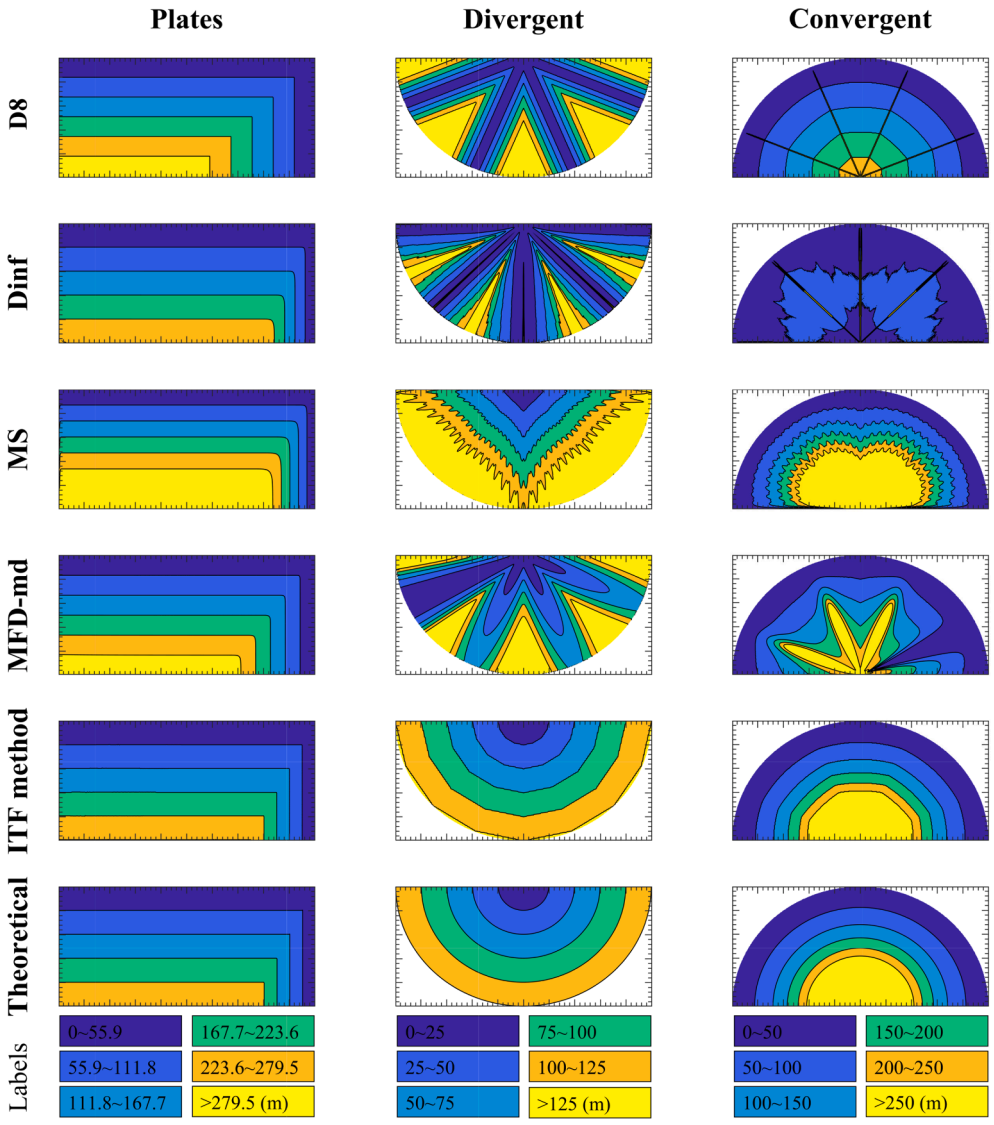

Fig. 7. Theoretical and extracted spatial patterns of slope length on three types of surfaces (planar style). According to Eq. 15, the theoretical maximum DWESL is 279.5, 125 and 31249.5 m on plate, divergent and convergent surface.s, respectively.

The algorithms D8 and Dinf, simulating water flow with an incomplete overflowing effect, may cause some cells on the divergent surface to lose the source of upstream water. These spatial patterns of slope length are thus discontinuous (Fig. 7). The results extracted using MS can fully cover the entire region on the divergence surface, because the model can simulate multidirectional fully divergent flow but can also lead to larger cumulative results. The performance on the divergent surface is similar for MFD-md and D8, but MFD-md's spatial patterns are less volatile due to the cross-compensation in multiple directions. In the ITF method, each cell can be ensured to be allocated to the local highest point along the uphill slope line, which can effectively overcome the shortcomings of SFD and achieve results similar to the theoretical value.

D8 and Dinf can effectively aggregate into a rill in the flow-gathering area while ignoring the overflow before the channel is formed. In the convergent surface shown in Fig. 5g, only the lowest point in the inward cone is the final destination of all flows. MS and the ITF method can effectively simulate this situation, and MFD-md can take into account both divergence and aggregation. As k_c gradually decreases (< 0) and *l*increases in the convergent area, the gathering speed of water flow increases, the cumulative value of the slope length becomes larger and the corresponding flow erosion is worse.

The difference between these conventional algorithms (D8, Dinf, MS and MFD-md) is mainly due to the different flow strategies assigned by each cell to the neighbors. These flow-simulation algorithms are designed based on the assumption of flow pattern, with different complexities and accuracies of calculation (Table 2). The RRMSE ranking of extraction results of each method was in the order ITF method <Dinf <MFD-md <D8 <MS on the plates, ITF method <MFD-md <MS <Dinf <D8 on the divergent surfaces and ITF method <MS <MFD-md <Dinf <D8 on the convergent surfaces.

Table 2
RRMSE between the extraction results of the methods and the theoretical values on synthetic surfaces.

Synthetic surfaces		D8	Dinf	MS	MFD-md	ITF
Plate	Planar	0.2416	0.0793	0.5006	0.1813	**0.0630**
	Concave	0.2416	0.0799	0.5007	0.1820	**0.0613**
	Convex	0.2416	0.0794	0.5006	0.1820	**0.0611**
Divergent	Planar	0.8112	0.6187	0.5746	0.5180	**0.0145**
	Concave	0.8110	0.6155	0.5774	0.5192	**0.0145**
	Convex	0.7598	0.6174	0.5437	0.5153	**0.0152**
Convergent	Planar	2.7562	2.2874	0.4057	0.6412	**0.0967**
	Concave	2.7582	2.2785	0.4041	0.6405	**0.0948**
	Convex	2.7601	2.3440	0.4080	0.6427	**0.0949**

For each method, the RRMSE of DWESL extracted from the planar, concave and convex surfaces are highly similar within the same type (Table 2). The differences between the three styles of each type are mainly due to the change in elevation, and the differences of the weights of flow distribution of the cells leads to the slight differences of the final result. In the ITF method, the performance of the up_iGD8 algorithm on planar, concave and convex surfaces differs slightly (Wu et al., 2020). The error for *l*and the piecewise calculation based on the approximate solution Eq. 11 also affect the final result.

4.1.2. *Extracted slope lengths on Himmelblau-Orlandini surfaces*

The spatial pattern extracted by each method indicated that the results of D8 and Dinf were fragmented and discontinuous (Fig. 8a, Fig. 8b). MFD-md can be regarded as an enhancement of D8 (Fig. 8d), and cross-compensation in multiple directions can reduce the loss of upstream water to some cells. Compared with MS, MFD-md can effectively gather into rills in the convergence region. The results of MS and the ITF method can correspond to the surface structure to a large extent (Fig. 8c, Fig. 8e), but the ITF method is more consistent with numerical transitions of the structure of terrain surfaces.

The cumulative frequency curve of slope length in the divergent area ($k_c > 0$) (Fig. 9) indicated that 95% of the DWESLs extracted using D8, Dinf, MS, MFD-md and the ITF method were <123.8, 100.5, 129.8, 119.5 and 95.1 m, respectively. The proportions of the DWESLs <15 m for D8, Dinf, MS, MFD-md and the ITF method were 20.1, 27.4, 4.5, 13.3 and 8.4%, respectively. D8 and Dinf had more low values than the other methods due to the outflow of each cell in one or two directions, so some cells lost upstream water in the divergent region. The average slope length extracted using the Dinf method was therefore lowest (Table 3). In the ITF method, the minimum slope length was much smaller than a CSL of these algorithms simulating conventional flow, because k_c at the ridge or local highest position is larger and l is smaller, which also accounted for why the slope length of these methods was overestimated in strongly divergent areas (Gallant and Hutchinson, 2011). Among the results of 22 sample points, the error was lowest with the ITF method (Fig. 10b, Fig. 10c), because up_iGD8 provided a reliable direction that matched the exact slope line well (Fig. 10a).

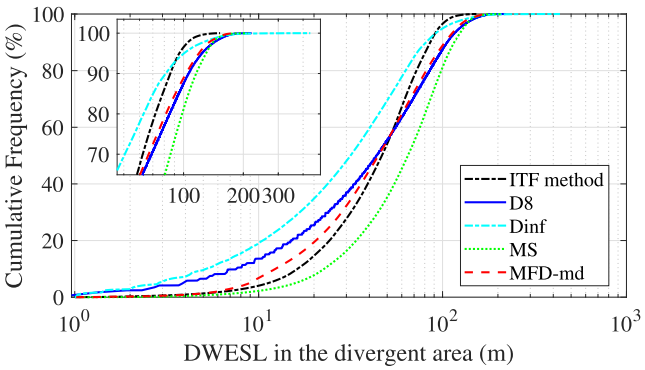

Fig. 9. Curves of the cumulative frequency of slope length in the divergent area on the Himmelblau-Orlandini surface extracted using the five methods.

Table 3
Information for the numerical distribution of slope length in the divergent area of the Himmelblau-Orlandini surface.

	D8	Dinf	MS	MFD-md	ITF
Max (m)	220.10	434.87	209.97	182.64	152.73
Min (m)	0.96	1.00	1.06	1.00	0.18
Mean (m)	51.41	39.07	67.33	52.06	48.99
Std.	38.45	32.95	35.08	34.75	26.29

4.2. *Extracted DWESL on real terrain data*

The spatial distributions of DWESL were 'smoother' (Fig. 11c, d, e) using MS, MFD-md and the ITF method than D8 and Dinf (Fig. 11a, Fig. 11b), indicating less-abrupt variations in the magnitude of slope length for adjacent cells. The performance of D8 could not accurately represent the complex terrain convergence, and the spatial patterns of Dinf were the most fragmented. The MFD-md result was more concentrated in the convergence region than that of MS. The spatial distribution of the ITF method was very similar to that of MFD-md, but the DWESLs of these flow-simulation methods were larger than that of the ITF method in the areas with strong divergence (e.g. ridges and hilltops). The root cause of these differences was the corresponding calculation

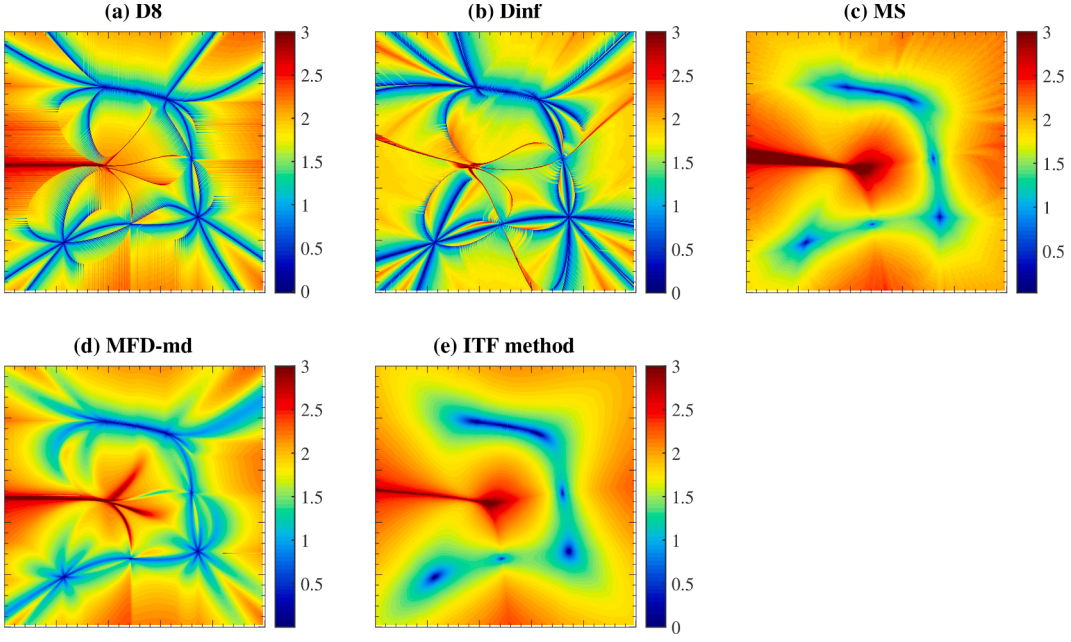

Fig. 8. Spatial patterns of logarithmic slope lengths limited to ⩽1000 m extracted using the five methods.

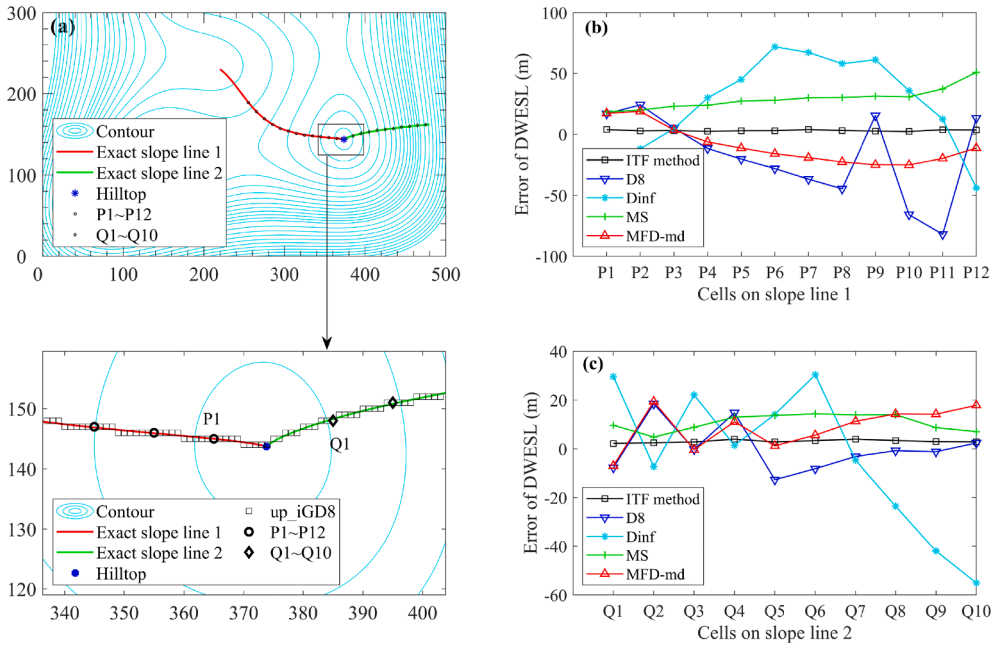

Fig. 10. Errors of DWESL on the Himmelblau-Orlandini surface extracted using the five methods. (a) Local magnification of selected slope lines and sample points. (b) Error of DWESL extracted using the five methods at sample points on slope line 1. (c) Error of DWESL extracted using the five methods at sample points on slope line 2.

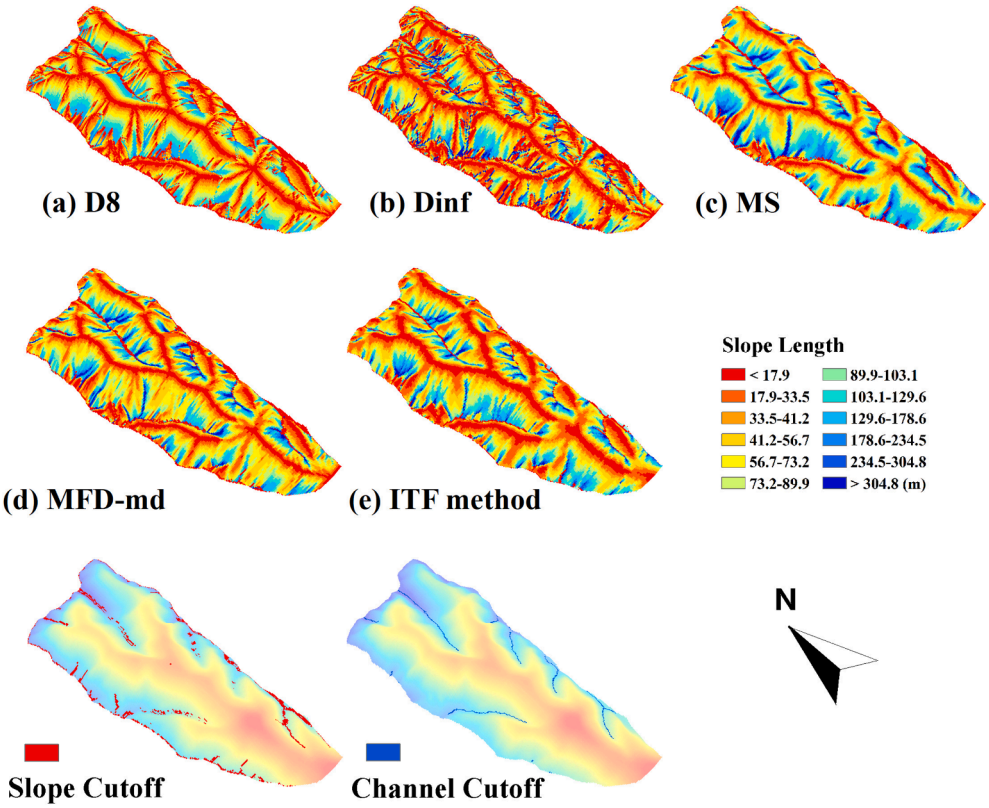

Fig. 11. Spatial pattern of DWESL on real terrain extracted by five methods, with the same cutoff factors. (slope cutoff factor threshold: the change in gradient is 70% when slope <2.86°, the change in gradient is 50% when slope ⩾2.86°; channel cutoff factor threshold: accumulated area >4000 m^2.

model of slope length. The spatial patterns of slope length shown in these maps indicated the potential risk of erosion, which was closely related to the surface structure. Ridges and hilltops were highly divergent, and the overland runoff and sediment were not transported along these drainage divides, but converged or diverged along the hillsides. Hence, the erosion risk was the lowest on drainage divides, and the erosion risk was related to the structure of divergence and convergence on hillsides. In terms of the two cutoff factors of slope length in Fig. 11, the depositions caused by the change of gradient occurred in small amounts on special hillsides, mostly occurred near the gullies, including

ephemeral creeks, permanent streams and large rivers. Channel cutoff factor in the model further limited the termination conditions of slope length, that was, a well-defined channel. Therefore, the risk of erosion was very high in some strongly converging area where the well-defined channel was not formed, and the numerical values of slope length have exceeded the quantitative significance (>1000ft, >304.8 m).

The cumulative frequency curves of the DWESLs (Fig. 12) indicated that 95% of the DWESLs were <144.8 m for D8, <260.3 m for Dinf, <241.6 m for MS, <210.8 m for MFD-md and <189.7 m for the ITF method. Ninety-five percent of the DWESLs for the ITF method were shorter than those for Dinf, MS and MFD-md but not D8, because the spatial pattern of D8 lost details in parts of the convergence area, inconsistent with the real terrain.

To summarize, the results extracted using the ITF method had the smallest errors on the synthetic surfaces and a more reasonable spatial pattern consistent with the terrain structure on all surfaces. Based on the premise of ensuring that each cell could be traced back to the hilltop along the uphill slope line, the contour curvature of the cell location and the uphill runoff length interacted with each other (Gallant and Hutchinson, 2011, para.32). l played an important role on the planar hillsides, l and k_c competed with each other on the divergent hillsides and the joint action of l and k_c affected the calculation of cumulative slope lengths on the convergent hillsides.

5. Conclusion

Based on the previous exploration of the methods for extracting slope length in USLE/RUSLE, this study has made further progress. The theoretical model of slope length was optimized from the continuous solution space of morphology. We combined the differential equation for SCA, and proposed ITF method for extracting slope length. Considering the topology and convenience of grid DEM, we used iGD8-based strategy avoiding the interpolation for grid DEM in ITF method. Unlike using conventional algorithms that simulate flow for calculating the uphill contributing area and the effective contour length of discrete elements for extracting slope length, the outputs of ITF method were prevented from being overestimated, especially in areas with strong divergence and cutoff positions. The spatial distribution of the extracted slope length was more consistent with the terrain than that of original method. The ITF method and the extracted slope length could be directly coupled to the L factor in USLE/RUSLE, which was convenient for application.

Nevertheless, there are still some problems that need to be researched in the future.

The determination of channel cutoff factor in the definition of slope length still needs to be further clarified and improved. Well-defined channels may be wide gullies, flat valleys, permanent rivers, etc., how to effectively determine these cutoff factors according to the field condition? Remote sensing images and field observation can only get relevant data at a specific time. Even so, quantitative calculation of channel width and identification of channel head were challenging. For DEM data with certain resolution, the channel network was required to further consider the actual channel width, not just a fixed width of pixel. In addition, some user-defined thresholds required expert experience, which made it difficult for large-scale erosion mapping.

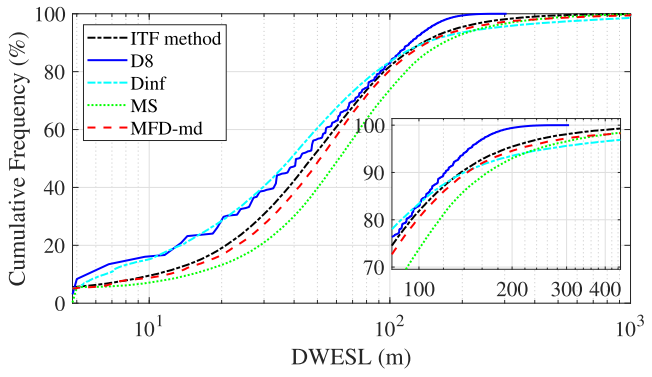

Fig. 12. Curves of the cumulative frequency of DWESL on real terrain extracted using the five methods.

With the ultimate goal of applying USLE/RUSLE for predicting average soil loss, the universality of the proposed method required to be tested on more field terrain. The main idea of this work was to verify the rationality and precision of the proposed method at the theoretical level. A set of accurate pixel erosion data would be expected to evaluate these automated GIS procedures, which put forward higher requirements for geodesy and metrology.

Declaration of Competing Interest

The authors declare that they have no known competing financial interests or personal relationships that could have appeared to influence the work reported in this paper.

Acknowledgment

The authors would like to express great appreciation to Yi Chang, Zhitong Sun, Yikun Xu, Hanghao Li and Tianyang Qiao for their discussion on the details of the experiment. Thanks to Dr. William Blackhall for language edition. This research was supported by National Natural Science Foundation of China (41771315), National key Research and Development Project (2020YFD1100601), EU Horizon 2020 research and innovation programme (ISQAPER: 635750).

References

Alexakis, D., Tampakopoulou, E., Grilllakis, M., Tsanis, I., 2019. Using satellite remote sensing and regional climate change scenario data for projecting soil erosion risk. a case study in crete, greece. In: IGARSS 2019–2019 IEEE International Geoscience and Remote Sensing Symposium.

Anjitha Krishna, P.R., Lalitha, R., Shanmugasundaram, K., Nagarajan, M., 2019. Assessment of topographical factor (ls-factor) estimation procedures in a gently sloping terrain. Journal of the Indian Society of Remote Sensing 47, 1031–1039.

Baghdad, B., Taoufik, M., Hadi, H.E., 2020. Soil erosin assessment in extraction area: abandonned quarries akreuch marocco. In: 2020 International conference of Moroccan Geomatics (Morgeo).

Bircher, P., Liniger, H.P., Prasuhn, V., 2019. Comparing different multiple flow algorithms to calculate rusle factors of slope length (l) and slope steepness (s) in switzerland. Geomorphology 346, 106850.

Brychta, J., Brychtová, M., 2020. Possibilities of including surface runoff barriers in the slope-length factor calculation in the gis environment and its integration in the user-friendly ls-rusle tool. Soil and Water Research 15, 246–257.

Costa-Cabral, M.C., Burges, S.J., 1994. Digital elevation model networks (demon): a model of flow over hillslopes for computation of contributing and dispersal areas. Water Resour. Res. 30, 1681–1692.

D. Moore, I., J. Burch, G., 1986. Modelling erosion and deposition: Topographic effects. Transactions of the ASAE 29, 1624–1630.

Desmet, P.J.J., Govers, G., 1996. A gis procedure for the automated calculation of the usle ls factor on topographically complex landscape units. J. Soil Water Conserv. 51, 427–433.

Desmet, P.J.J., Govers, G., 1997. Comment on 'modelling topographic potential for erosion and deposition using gis'. International Journal of Geographical Information Science 11, 603–610.

Foster, G.R., Wischmeier, W.H., 1974. Evaluating irregular slopes for soil loss prediction. Trans American Society of Agricultural Engineers 17, 305–309.

Fu, S., Wu, Z., Liu, B., 2013. Comparison of the effects of the different methods for computing the slope length factor at a watershed scale. International Soil & Water Conservation Research 1, 64–71.

Gallant, J.C., Hutchinson, M.F., 2011. A differential equation for specific catchment area. Water Resources Research 47.

Garcia Rodriguez, J.L., Gimenez Suarez, M.C., 2012. Methodology for estimating the topographic factor ls of rusle3d and usped using gis. Geomorphology 175, 98–106.

Hickey, R., 2000. Slope angle and slope length solutions for gis. Cartography 29, 1–8.

Hickey, R., Smith, A., Jankowski, P., 1994. Slope length calculations from a dem within arc/info grid. Comput. Environ. Urban Syst. 18, 365–380.

Hrabalíková, M., Janeek, M., 2017. Comparison of different approaches to ls factor calculations based on a measured soil loss under simulated rainfall. Soil & Water Research 12, 69–77.

Liu, B., Zhang, K., Xie, Y., 2002. An empirical soil loss equation. In: Process of 12th international soil conservation organization conference, Beijing, China, pp. 143–149.

López-Vicente, M., González-Romero, J., Lucas-Borja, M., 2020. Forest fire effects on sediment connectivity in headwater sub-catchments: Evaluation of indices performance. Science of The Total Environment 732, 139206.
Mitasova, H., Hofierka, J., 1993. Interpolation by regularized spline with tension: Ii. application to terrain modeling and surface geometry analysis. Math. Geol. 25, 657–669.
Mitasova, H., Hofierka, J., Zlocha, M., Iverson, L.R., 1996. Modelling topographic potential for erosion and deposition using gis. International Journal of Geographical Information Systems 10, 629–641.
Moore, I.D., Wilson, J.P., 1992. Length-slope factors for the revised universal soil loss equation: Simplified method of estimation. J Soil & Water Conservation 47, 423–428.
O'Callaghan, J.F., Mark, D.M., 1984. The extraction of drainage networks from digital elevation data. Computer Vision Graphics & Image Processing 27, 323–344.
Orlandini, S., Moretti, G., Franchini, M., Aldighieri, B., Testa, B., 2003. Path-based methods for the determination of nondispersive drainage directions in grid-based digital elevation models. Water Resour. Res. 39, 1144–1151.
Orlandini, S., Moretti, G., Gavioli, A., 2014. Analytical basis for determining slope lines in grid digital elevation models. Water Resour. Res. 50, 526–539.
Panagos, P., Borrelli, P., Meusburger, K., 2015. A new european slope length and steepness factor (ls-factor) for modeling soil erosion by water. Geosciences 5, 117–126.
Paz, A.R., Collischonn, W., Risso, A., Mendes, C.A.B., 2008. Errors in river lengths derived from raster digital elevation models. Computers & Geosciences 34, 1584–1596.
Pilesjö, P., Hasan, A., 2014. A triangular form-based multiple flow algorithm to estimate overland flow distribution and accumulation on a digital elevation model. Transactions in GIS 18, 108–124.
Qin, C., Zhu, A., Pei, T., Li, B., Zhou, C., Yang, L., 2007. An adaptive approach to selecting a flow-partition exponent for a multiple-flow-direction algorithm. International Journal of Geographical Information Science 21, 443–458.
Qin, C.Z., Ai, B.B., Zhu, A.X., Liu, J.Z., 2017. An efficient method for applying a differential equation to deriving the spatial distribution of specific catchment area from gridded digital elevation models. Computers & Geosciences 100, 94–102.
Qin, C.Z., Bao, L.L., Zhu, A.X., Hu, X.M., Qin, B., 2013. Artificial surfaces simulating complex terrain types for evaluating grid-based flow direction algorithms. International Journal of Geographical Information Science 27, 1055–1072.
Quinn, P., Beven, K., Chevallier, P., Planchon, O., 1991. The prediction of hillslope flow paths for distributed hydrological modelling using digital terrain models. HYDROLOGICAL PROCESSES 5, 59–79.
Remortel, R.D.V., Hamilton, M.E., Hickey, R.J., 2001. Estimating the ls factor for rusle through iterative slope length processing of digital elevation data within arclnfo grid. Surveyor 30, 27–35.
Remortel, R.D.V., Maichle, R.W., Hickey, R.J., 2004. Computing the ls factor for the revised universal soil loss equation through array-based slope processing of digital elevation data using a c++ executable. Computers & Geosciences 30, 1043–1053.
Renard, K.G., Foster, G.R., Weesies, G.A., Porter, J.P., 1991. Rusle: Revised universal soil loss equation. J Soil & Water Conservation 46.
Shary, P.A., 1995. Land surface in gravity points classification by a complete system of curvatures. Math. Geol. 27, 373–390.
Shin, S., Paik, K., 2017. An improved method for single flow direction calculation in grid digital elevation models. Hydrol. Process. 31, 1650–1661.
Tarboton, D.G., 1997. A new method for the determination of flow directions and upslope areas in grid digital elevation models. Water Resour. Res. 33, 309–319.
Wang, C., Shan, L., Liu, X., Yang, Q., Cruse, R.M., Liu, B., Li, R., Zhang, H., Pang, G., 2020. Impacts of horizontal resolution and downscaling on the usle ls factor for different terrains. International Soil and Water Conservation Research 8, 363–372.
Wang, C., Yang, Q., Pang, G., Wen, B., 2016. Assessment of 1 arcsec srtm data quality in china taking loess hilly area as an example. In: Igarss IEEE International Geoscience and Remote Sensing Symposium.
Wechsler, S.P., Kroll, C.N., 2006. Quantifying dem uncertainty and its effect on topographic parameters. Photogrammetric Engineering and Remote Sensing 72, 1081–1090.
Winchell, M.F., Jackson, S.H., Wadley, A.M., Srinivasan, R., 2008. Extension and validation of a geographic information system-based method for calculating the revised universal soil loss equation length-slop factor for erosion risk assessments in large watersheds. J. Soil Water Conserv. 63, 105–111.
Wischmeier, W.H., Smith, D., 1978. Predicting rainfall erosion losses: A guide to conservation planning with Universal Soil Loss Equation (USLE). U.S. Department of agriculture, Washington,D C.
Wu, P., Liu, J., Han, X., Liang, Z., Liu, Y., Fei, J., 2020. Nondispersive drainage direction simulation based on flexible triangular facets. Water Resources Research 56.
Yadav, S., Indu, J., 2016. Estimation of vertical accuracy of digital elevation models over complex terrains of indian subcontinent. In: IGARSS 2016–2016 IEEE International Geoscience and Remote Sensing Symposium.
Yan, Y., Tang, J., Pilesjö, P., 2018. A combined algorithm for automated drainage network extraction from digital elevation models. Hydrol. Process. 32, 1322–1333.
Yang, Q.K., Vicar, M., Niel, T.G.V., Hutchinson, M.F., Li, L.T., Zhang, X.P., 2007. Improving a digital elevation model by reducing source data errors and optimising interpolation algorithm parameters: An example in the loess plateau, china. Int. J. Appl. Earth Obs. Geoinf. 9, 235–246.
Yang, X.H., 2015. Digital mapping of rusle slope length and steepness factor across new south wales, australia. Soil Research 53, 216–225.
Zhang, H., Wei, J., Yang, Q., Baartman, J.E.M., Geissen, V., 2017. An improved method for calculating slope length (λ) and the ls parameters of the revised universal soil loss equation for large watersheds. Geoderma 308, 36–45.
Zhang, H., Yang, Q., Li, R., Liu, Q., Moore, D., He, P., Ritsema, C.J., Geissen, V., 2013. Extension of a gis procedure for calculating the rusle equation ls factor. Computers & Geosciences 52, 177–188.
Zhang, H., Yao, Z., Yang, Q., Li, S., Baartman, J.E.M., Gai, L., Yao, M., Yang, X., Ritsema, C.J., Geissen, V., 2017. An integrated algorithm to evaluate flow direction and flow accumulation in flat regions of hydrologically corrected dems. Catena 151, 174–181.
Zhou, Q., Liu, X., 2002. Error assessment of grid-based flow routing algorithms used in hydrological models. International Journal of Geographical Information Science 16, 819–842.
Zhu, Q., Yang, X., Qiang, Y., 2016. Assess the topographic resolution impact on soil loss. In: IGARSS 2016–2016 IEEE International Geoscience and Remote Sensing Symposium.
Zhu, S., Tang, G., Xiong, L., Zhang, G., 2014. Uncertainty of slope length derived from digital elevation models of the loess plateau, china. Journal of Mountain Science 11, 1169–1181.